Atmos. Chem. Phys. Discuss., 15, 4219–4263, 2015
www.atmos-chem-phys-discuss.net/15/4219/2015/
doi:10.5194/acpd-15-4219-2015

Atmospheric Chemistry and Physics Discussions

Model studies of volatile diesel exhaust particle formation: organic vapours involved in nucleation and growth?

L. Pirjola[1,2], M. Karl[3], T. Rönkkö[4], and F. Arnold[5,6]

[1]Department of Technology, Metropolia University of Applied Sciences, P.O. Box 4021, 00180 Helsinki, Finland
[2]Department of Physics, University of Helsinki, P.O. Box 64, 00014 Helsinki, Finland
[3]Norwegian Institute for Air Research, P.O. Box 100, 2027 Kjeller, Norway
[4]Aerosol Physics Laboratory, Department of Physics, Tampere University of Technology, P.O. Box 692, 33101 Tampere, Finland
[5]Max-Planck-Institut für Kernphysik, Heidelberg, Germany
[6]Deutsches Centrum für Luft and Raumfahrt (DLR), Obenpfaffenhofen, Germany

Received: 2 November 2014 – Accepted: 30 January 2015 – Published: 17 February 2015

Correspondence to: L. Pirjola (liisa.pirjola@metropolia.fi, liisa.pirjola@helsinki.fi)

Published by Copernicus Publications on behalf of the European Geosciences Union.

Abstract

High concentration of volatile nucleation mode particles (NUP) formed in the atmosphere during exhaust cools and dilutes have hazardous health effects and impair visibility in urban areas. Nucleation mechanisms in diesel exhaust are only poorly understood. We performed model studies using two sectional aerosol dynamics process models AEROFOR and MAFOR on the formation of particles in the exhaust of a diesel engine, equipped with an oxidative after-treatment system and running with low fuel sulphur content (FSC), under laboratory sampling conditions where the dilution system mimics real-world conditions. Different nucleation mechanisms were tested; based on the measured gaseous sulphuric acid (GSA) and non-volatile core and soot particle number concentrations of the raw exhaust, the model simulations showed that the best agreement between model predictions and measurements in terms of particle number size distribution was obtained by barrierless heteromolecular homogeneous nucleation between GSA and semi-volatile organic vapour (for example adipic acid) combined with the homogeneous nucleation of GSA alone. Major growth of the particles was predicted to occur by the same organic vapour at concentrations of $(1-2)\times10^{12}\,\mathrm{cm}^{-3}$. The pre-existing core and soot mode concentrations had opposite trend on the NUP formation, and maximum NUP formation was predicted if a diesel particle filter (DPF) was used. On the other hand, NUP formation was ceased if the GSA concentration was less than $10^{10}\,\mathrm{cm}^{-3}$ which suggests, based on the measurements, the usage of biofuel to prevent volatile particles in diesel exhaust.

1 Introduction

Regardless of many improvements in vehicle technology exhaust particles emitted from traffic constitute major air pollutants in urban environments. Although, due to the tightened emission regulations, the mass emissions of diesel particles have been reduced, the number emission of exhaust nanoparticles has been reported to be significant

ACPD
15, 4219–4263, 2015

(Rönkkö et al., 2013; Lähde et al., 2010). These non-regulated particles can penetrate deepest into the human pulmonary and blood-vascular systems having hazardous health effects (Pope and Dockery, 2006; Sioutas et al., 2005; Kettunen et al., 2007, Su et al., 2008; Alföldy et al., 2009). Exhaust particles also affect climate by scattering or absorbing solar radiation and participating in cloud formation (Charsson et al., 1992; Bond et al., 2013).

The major source of diesel particulate mass is the soot mode. These particles, with sizes of 40–100 nm, are formed in the combustion process and are composed of non-volatile carbonaceous soot agglomerates, onto which semivolatile vapours can condense (e.g. Kittelson, 1998; Tobias et al., 2001). The Euro 6 level diesel vehicles are equipped with diesel particle filters (DPF) or partial diesel particle filters (pPDF) (Heikkilä et al., 2009) which remove totally or partly the soot particles. The oxidative after-treatment systems such as diesel oxidising catalyst (DOC) reduce exhaust hydrocarbon concentrations but simultaneously increase SO_2 to SO_3 conversion enhancing gaseous sulphuric acid (GSA) formation (Arnold et al., 2006, 2012; Maricq et al., 2002). The GSA has a very low saturation vapour pressure, and it has been shown to participate in condensation and nucleation processes during the dilution and cooling of the exhaust (Arnold et al., 2006, 2012; Rönkkö et al., 2013; Shi and Harrison, 1999; Tobias et al., 2001; Schneider et al., 2005; Khalek et al., 2003). These nucleation mode particles are volatile consisting of sulphate and hydrocarbons (Kittelson, 1998). With some vehicle technologies and in some driving conditions, non-volatile nanoparticles around 10 nm or less have been observed. These particles are suggested to be formed by fuel aliphatic hydrocarbons (Filippo et al., 2008) or lubricant oil metal compounds (Kittelson et al., 2008; Rönkkö et al., 2013; Karjalainen et al., 2014) coated by condensing volatile hydrocarbon and sulphur compounds (Rönkkö et al., 2007, 2013).

Although the measurements indicate that sulphuric acid participates in the production of volatile exhaust particles, the nucleation mechanism is not known. Numerous different nucleation theories involving sulphuric acid such as homogeneous binary nucleation (BHN) (Kulmala et al., 1998; Vehkamäki et al., 2002, 2003), ternary nucleation

ACPD
15, 4219–4263, 2015

(Napari el al., 2002; Merikanto et al., 2007), activation nucleation (Kulmala et al., 2006), kinetic nucleation (Weber et al., 1997), ion-induced nucleation (Raes et al., 1985; Arnold et al., 1999; Yu and Turco, 2000), and recently sulphuric acid-amine nucleation (Almeida et al., 2013) have been proposed to explain nucleation bursts under atmospheric conditions. Because vehicle exhaust includes similar species than the atmosphere, NUP formation might occur in the same way. Arnold et al. (1999) have actually made mass spectrometric measurements of chemi-ions present in the exhaust of combustion engines, including car engines and aircraft gas turbine engines. On the other hand, Ma et al. (2008) reported that ion-induced nucleation did not play an important role in the NUP formation in diesel exhaust. Ion-induced nucleation is not considered in this work.

Recently published models simulating the formation and growth of exhaust particles can be divided into two groups, some of them are process models (Shi and Harrison, 1999; Voutsis et al., 2005; Lemmetty et al., 2008; Hu and Yu, 2006, 2008) as is also the model considered in this paper. Some are computational fluid dynamics (CFD) models coupled with aerosol dynamics (Uhrner et al., 2007; Albriet et al., 2010; Liu et al., 2011) and furthermore with the major turbulent mixing processes (Wang and Zhang, 2012).

Shi and Harrison (1999) concluded that the BHN predicted several orders of magnitude lower nucleation rates than those measured even though the fuel sulphur content (FSC) was as high as 300–500 ppm, and no sink processes such as condensation and coagulation were taken into account. The simulation results reported by Voutsis et al. (2005) showed that the barrierless nucleation scheme could predict the NUP concentration rather well for high sulphur fuel (FSC = 250 ppm) whereas the nucleation rate proportional to the square of sulphuric acid saturation vapour pressure was appropriate for ultra-low sulphur fuel (FSC = 10 ppm). Lemmetty et al. (2008) found that by assuming the high SO_2 to SO_3 conversion ratio of 90 %, BHN nucleation reproduced the measured size distributions opposed to barrierless nucleation. Du and Yu (2006) concluded that by using their kinetic BHN model for the vehicles running on the fuel with the FSC of 330 ppm, the BHN scheme could not predict the measured NUP con-

ACPD
15, 4219–4263, 2015

centrations if the SO_2 to SO_3 conversion ratio was 1 %, but that it was appropriate for the ratios greater than 4 % even though FCS was less than 50 ppm. If the FSC was 15 ppm, the BHN was the main source of NUP only for vehicles equipped by continuously regenerating particle filters (Du and Yu, 2008).

All of these studies indicate that other low or semi-volatile condensable vapours than GSA are required to explain the measured particle number size distributions. However, all of the previous model studies suffer from the lack of the GSA measurements. It is well-known that even a small change in the GSA concentration can cause several orders of magnitude difference in the binary nucleation rate.

The main objective of this paper is to quantify the relevant nucleation mechanism and the concentration of a semi-volatile condensable organic vapour (COV) to explain the diesel particle evolution in an ageing chamber under laboratory conditions which mimic well the atmospheric dilution conditions. For the first time the applicability of nucleation between an organic compound and sulphuric acid in diesel exhaust is investigated. The other objective is to investigate how changes in vehicle after-treatment technologies, fuel and lubricant oil affect exhaust particle nucleation and growth.

The model simulations are performed by an aerosol dynamics model AEROFOR (e.g. Pirjola, 1999; Pirjola and Kulmala, 2001; Lemmetty et al., 2008; Arnold et al., 2012). The GSA and particle concentrations in the raw exhaust were adopted from the measurements by Arnold et al. (2012) and Rönkkö et al. (2013). The first model simulations for the same engine equipped with the DOC and DPF we have already described in Arnold et al. (2012). Since AEROFOR produces only the time evolution of the particle number size distributions and concentrations, some of the simulations were repeated with another aerosol dynamics model MAFOR (Karl et al., 2011) which is able to produce the mass and composition size distributions of a multicomponent aerosol.

Both models, AEROFOR and MAFOR, are Lagrangian type box models which are well established and evaluated. Although these models are not able to give spatial distribution of temperature and aerosol scalars in the sampling system (Olin et al.,

ACPD
15, 4219–4263, 2015

2014), they were able to achieve the goals of this study, and subsequently increase our understanding on the formation and transformation mechanisms in diesel exhaust under laboratory and atmospheric conditions.

2 Methods

2.1 Sampling system and measurements

Since the detailed description of the measurements and instrumentation can be found in Arnold et al. (2012) and Rönkkö et al. (2013), only a short description relevant to the modelling point of view is given here. The emission measurements of a Euro IV standard heavy duty diesel engine were performed on an engine dynamometer. Four steady-state conditions with engine loads of 100, 75, 50 and 25 % were studied. The FSC was 36 ppm, additionally the FSC of 6 ppm was used in some experiments. Different after-treatment systems were used, this work mainly deals with the cases when the engine was equipped with DOC and pDPF.

The particle sampling and dilution system was a modified version of partial flow sampling system (Ntzhiachristos et al., 2004) and similar to that used e.g. by Vaaraslahti et al. (2005) and Rönkkö et al. (2006). It has been shown to mimic the real-world particle formation and growth processes relatively well (Gieschaskiel et al., 2005; Rönkkö et al., 2006). The sampling system consisted of a porous tube type primary diluter followed by an aging chamber and an ejector type diluter (Fig. 1).

The ageing chamber was used to ensure adequate residence time for the condensational growth of the nucleation mode particles in the cooled and diluted aerosol sample. The following ejector diluter was used to bring the sample into the ambient pressures and to ensure that the particle number concentration was in the measurement range of particle measurement equipment, without significant effect on particles formed during exhaust dilution and cooling (Giechaskiel et al., 2009). In the primary diluter, dilution air temperature was 30 °C, relative humidity close to zero and the dilution ratio was kept at

ACPD
15, 4219–4263, 2015

12. The dilution ratios were calculated from the measured CO_2 concentrations of the diluted exhaust sample and the raw exhaust. Based on the constant exhaust flow rate in the dilution and sampling system (55 lpm) and the measures mentioned in Fig. 1, the residence time of the exhaust in the tube between the PD and AC was 0.1 s and in the ageing chamber 2.6 s. Furthermore, exhaust temperature was measured at two points marked in Fig. 1.

Particle number size distributions of the exhaust were measured using two scanning mobility particle sizers (SMPS) measuring the particle diameters 3–60 nm and 10–430 nm. Also measured were the size distributions for all engine loads by using a thermodenuder TD in which the volatile material was evaporated at 265 °C temperature. The size distributions were corrected for particle losses in both SMPS and thermodenuder (Heikkilä et al., 2009).

The gaseous sulphuric acid GSA was monitored by a CIMS (Chemical Ion Mass Spectrometer) whose setup consists of a flow tube reactor through which is passed the exhaust plume. Details of the instrument can be found in Fiedler et al. (2005) and Arnold et al. (2012). Additionally, the acidic trace gases were measured in a way analogous to GSA.

2.2 Model descriptions

Model simulations were performed by a slightly updated version of an atmospheric chemistry and aerosol dynamics box model AEROFOR (e.g. Pirjola, 1999; Pirjola and Kulmala, 2001; Pirjola et al., 2004; Arnold et al., 2012). The model includes gas phase chemistry, formation of thermodynamically stable clusters by different nucleation mechanisms, condensation of H_2SO_4, H_2O and an organic vapour onto particles (Fuchs and Sutugin, 1970) taking into account molecular dimensions (Lehtinen and Kulmala, 2003), Brownian coagulation of particles (Fuchs, 1964), temperature and cooling profiles (Lemmetty et al., 2006), wall losses (Voutsis et al., 2005) as well as mixing with the particle-free dry diluted air.

ACPD
15, 4219–4263, 2015

In this study, four nucleation mechanisms are used: (1) classical binary homogeneous H_2SO_4–H_2O nucleation (BHN) (Vehkamäki et al., 2003), (2) activation theory (ACT) (Kulmala et al., 2006) where under the steady state nucleation rate the number of activated clusters is linearly proportional to the sulphuric acid concentration. ie. the nucleation rate $J = A[H_2SO_4]$ (A = activation coefficient), (3) kinetic nucleation (KIN) (McMurry and Friedlander, 1979; Weber et al., 1997; Sihto et al., 2006), where homogeneous homomolecular nucleation occurs involving two sulphuric acid molecules and thus the nucleation rate J is proportional to the square of the sulphuric acid, i.e. $J = K[H_2SO_4]^2$ (K = kinetic coefficient which includes the collision frequence and the probability of formation of a stable particle after the collision), (4) homogeneous homomolecular nucleation of sulphuric acid along with homogeneous heteromolecular nucleation betweeen sulphuric acid and organic vapour molecules (HET) (Paasonen et al., 2010), i.e. $J = K_1[H_2SO_4]^2 + K_2[H_2SO_4][COV]$. The diameter of the nucleated particle was assumed to be 1.5 nm (Kulmala et al., 2007).

Condensable organic vapours (COV) are not yet identified, however, the CIMS results indicated that a good candidate might be adipic acid although its concentration could not be accurately measured. We have used adipic acid as a representative of all COVs. Besides condensation, adipic acid was also assumed to participate in heteromolecular nucleation. The thermodynamical properties of adipic acid were adopted from the literature (Bilde et al., 2003). The vapour concentration is a free parameter. Pure adipic acid is insoluble in water. Hämeri et al. (2002) have measured that organic fraction of the mixtures containing adipic acid and ammonium sulphate does not contribute to water uptake. However, Yeung et al. (2009) found that adipic acid can have effects similar to those of more water-soluble organic species. Since the AEROFOR model assumes that the particles are in balance with the ambient water vapour concentrations it might overestimate the wet diameter of the particles.

To minimise the effect of numerical diffusion, typical for sectional models, 100 size sections turned out to be sufficient. Sectional presentation for aerosol size distribution was used since this method is more advantageous for the treatment of simultaneous

ACPD
15, 4219–4263, 2015

nucleation and particle transformation than modal aerosol representations. Especially in diesel exhaust, rapid formation of volatile particles will lead to size distribution peaks that do not have lognormal shape.

The set of stiff differential equations describing the time evolution of the particle number concentrations in each section as well as the vapour concentrations was solved using Numerical Algorithms Group, Ltd. library FORTRAN-routine D02EJF (Numerical Algorithms Group, 1990). The time step was set to 0.01 s.

Some of the cases simulated by AEROFOR were repeated by a Multicomponent Aerosol Dynamic model MAFOR (Karl et al., 2011). The model describes aerosol formation via different nucleation processes (details on nucleation options in Karl et al., 2012a), here only the HET nucleation option was used. Further aerosol processes are condensation of H_2SO_4, H_2O, adipic acid and an extremely low-volatile vapor (ELVOC, represented by the *n*-alkane $C_{34}H_{70}$) as well as Brownian coagulation, and mixing with the particle-free dry diluted air. Mass transfer of gas molecules to particles is calculated using the Analytical Predictor of Condensation scheme (Jacobson, 1997). The composition of particles in any size bin can change with time due to multicomponent condensation and/or due to coagulation of particles. Thus the size-segregated chemical composition of the generated particulate matter can be tracked at high temporal resolution. MAFOR has been evaluated with chamber data (Karl et al., 2012b), particle number measurements at a motorway (Keuken et al., 2012), and it has been shown to compare well with AEROFOR (see Karl et al., 2011). In this study, 120 size bins were used to represent the aerosol size distribution ranging from 1.5 nm to 10 µm diameter. Effective density of 1200 kg m^{-3} (Virtanen et al., 2002) was used for soot particles.

2.3 Input values based on the measurements

In the model simulations with AEROFOR and MAFOR the raw exhaust dilutes rapidly by dry air (T = 303 K) so that the final dilution ratio DR_f is 12. Because it is very difficult to analyse mathematically the dilution and cooling processes we describe them with simple parameters as in Lemmetty et al. (2006). A detailed simulation of cluster and

ACPD
15, 4219–4263, 2015

particle formation during cooling in a porous diluter is out of the scope of this paper (see e.g. Pyykönen et al., 2007; Olin et al., 2014). According to Lemmetty et al. (2006), the temperature was assumed to follow the exponential curve of the Newtonian cooling

$$T(t) = T_{\text{fin}} + (T_1 - T_{\text{fin}}) \exp\left(-\frac{t}{\tau_c}\right) \quad (1)$$

where T_1 is the raw exhaust temperature and T_{fin} the final exhaust temperature. The parameter τ_c is time constant for cooling, and it is the time when the remaining excess temperature is ~ 37 % (= 1/e %) of the original value. In this work, τ_c was determined based on the temperature measurements at two points shown in Fig. 1, and a value of 0.03 s was obtained at all engine loads. Similarly to Lemmetty et al. (2006), dilution can be modelled by using an exponential equation

$$\text{DR}(t) = \text{DR}_f^{1/\tau_d}, t < \tau_d \quad (2)$$

Dilution time constant τ_d is the time in which the system has achieved the final dilution ratio, no dilution occurs after this. In this work τ_d is a free parameter. Its value was assumed to be 0.12 s; however, sensitivity tests will be presented in Sect. 3.3.1. It should be noted that by assuming that all cooling is caused by only dilution the upper limit for τ_c is determined by an equation (Lemmetty et al., 2006)

$$\tau_c \leq \frac{\tau_d}{\ln(\text{DR}_f)}. \quad (3)$$

Consequently, τ_d must be ≥ 0.075 s.

The initial exhaust particle size distribution (raw exhaust) accounted for two modes, the soot mode and the non-volatile core mode, both formed in the combustion processes in the engine. The modal geometric mean diameters (D_g), number concentrations and SDs (Table 1) were adopted from the measurements (Rönkkö et al., 2013).

The initial raw exhaust GSA concentrations were as well adopted from the measurements (Arnold et al., 2012; Rönkkö et al., 2013). During the 100 % engine load periods

ACPD
15, 4219–4263, 2015

the GSA concentration varied from 2.2×10^9 to 3×10^{12} cm^{-3}, during the 75 % engine load period from 1.2×10^{11} to 3×10^{11} cm^{-3}, and during the 50 % period it was around $6 \times 10^{10} - 1 \times 10^{11}$ cm^{-3} (Fig. 2). The history of the after-treatment system (ATS) had a large effect on the concentrations, especially, during the first 100 % engine load the increasing trend in the GSA concentration indicates strong storage effect of sulphuric acid onto the walls of the ATS.

Model simulations were performed mainly at 100 % engine load phases even though some simulations were repeated at 75 and 50 % engine loads. The models were initiated by the measured GSA and non-volatile particle concentrations given in Table 1.

3 Results and discussion

3.1 Comparison of the nucleation mechanisms

3.1.1 Binary homogeneous nucleation

In the first set of model simulations the BHN mechanism was assumed. Figure 3a illustrates the evolution of the particle number concentration N_3, gas concentrations and nucleation rate, along with the particle number size distribution at the end of the simulation when the initial GSA concentration was 2×10^{12} cm^{-3}. This was the measured stabilized concentration at the end of the second 100 % engine load in Fig. 2. Also shown is the measured particle size distribution at the end of the ageing chamber (Fig. 3b black curve), and time development of the condensation sink CS (Fig. 3c).

Two features emerge from the figures. First, nucleation occurs very fast, it starts after 0.1 s just at the entrance of the ageing chamber, and reaches the momentary maximum value 3.0×10^9 cm^{-3} s^{-1} after 0.23 s. Nucleation is totally suppressed after one second if no condensable organic vapour is present, and somewhat faster, after 0.6 s, if the condensable organic vapour concentration is present with a concentration of 8×10^{12} cm^{-3}. Sulphuric acid concentration decreases first mainly by dilution, but

ACPD
15, 4219–4263, 2015

after 0.12 s nucleation and condensation are competing processes. The time evolution of the condensation sink (CS) (e.g. Pirjola et al., 1999; Kulmala et al., 2001) whose inverse is a measure of the lifetime of condensable vapour molecules in the exhaust is presented in Fig. 3c for the simulations with and without organic vapour. The initial CS is 3.5 s^{-1} based on the dry core and soot modes. Due to dilution it decreases during the first 0.17 s but then steeply increases up to a value of 8.0 s^{-1} as long as nucleation occurs, and after the suppression of nucleation slightly decreases as the number concentration decreases due to coagulation, even though condensation still grows the particles. For comparison, typical atmospheric CS values are in the range of 10^{-4} – 10^{-1} s^{-1}. The predicted GSA concentrations at the end of the ageing chamber are 1.2×10^8 cm^{-3} and 6×10^6 cm^{-3} without and with the condensable organic vapour, respectively. Unfortunately, these values cannot be compared with observations since only the raw exhaust GSA concentration was measured.

Second, the newly formed particles are not able to grow to the measured sizes by sulphuric acid. At the end of the simulation, the modelled geometric mean diameter of the nucleation mode is only 5.5 nm. To reach the measured modal mean value of 13.7 nm the COV concentration should be as high as 8×10^{12} cm^{-3}. Consequently, the concentration of particles smaller than 40 nm covering the grown volatile and non-volatile nucleation mode particles is much higher than the observed one (Fig. 3b), the modelled total particle concentration N_3 (2.9×10^8 cm^{-3}) strongly exceeds the measured value 8×10^6 cm^{-3}.

When the raw exhaust GSA concentration was 4.4×10^{11} cm^{-3}, AEROFOR predicted the maximum momentary nucleation rate of 3.9×10^4 cm^{-3} s^{-1} (Fig. S1). Although nucleation took 2.2 s, it was not able to produce enough new particles. The final modelled N_3 was 6.8×10^5 cm^{-3}, too small compared to the measured N_3 of 6.6×10^6 cm^{-3}. The sulphuric acid concentration was not sufficient to grow the nucleated particles to the measured 11.2 nm sizes. When increasing the COV concentration up to 1×10^{12} cm^{-3}, the mean diameter of the core mode was close to the measured 21 nm, however the

ACPD
15, 4219–4263, 2015

nucleation mode diameter (9 nm) was still too small. On the other hand, higher COV concentrations let the core mode particles grow too much.

When the measured raw exhaust GSA concentration was 1.53×10^{11} cm^{-3}, the model did not predict any newly formed particles. This is inconsistent with the measurements which showed that the volatile nucleation mode was present since the GSA concentration exceeded 1×10^{10} cm^{-3} (Fig. S2). Thus we can conclude that the BHN mechanism cannot explain the measurements.

3.1.2 Cluster activation and kinetic nucleation

The second set of simulations was performed by using the ACT mechanism for nine different initial GSA values selected from Fig. 2. The activation coefficient A and the adipic acid concentration were varied. The changes affected the particle size distributions at the end of the ageing chamber so that an increase in A increased the height of the nucleation mode whereas an increase in the adipic acid concentration shifted the nucleation mode to larger sizes and simultaneously slightly decreased the height of the mode. As an example, Fig. 4 presents the results for all nucleation mechanisms studied in this work for 100 % engine load when the GSA concentration was stabilised to 2.0×10^{12} cm^{-3}, and COV = 6×10^{11} cm^{-3}. Again in the case when no condensable organic vapour was present the nucleation mode and even the core mode did not sufficiently grow.

With the ACT mechanism nucleation is not suppressed and the formation of 1.5 nm clusters occurs during the whole simulation time 2.7 s (Fig. S3). The formed clusters were activated to grow by sulphuric and adipic acids, however, the growth by sulphuric acid alone was not sufficient (Fig. S3, dotted line). With the adipic acid condensation, the N_3 at the end of the ageing chamber was 9.3×10^6 cm^{-3}, close to the measured value 6.6×10^6 cm^{-3}. As seen from Fig. 4, the left side of the nucleation mode is higher compared to the measurements. The reason is continuous nucleation and subsequent growth of the newly formed particles. From measurements' perspective, the SMPS underestimates the concentration of the smallest particles (below diameter of 10 nm).

ACPD
15, 4219–4263, 2015

For the other initial GSA values, the model was able to predict the measured size distribution as well. The estimated COV concentration was close to 10^{12} cm^{-3} except in the cases when practically no nucleation occurred, i.e. for the GSA concentration smaller than around 10^{10} cm^{-3}. It is not expected that the activation coefficient A was not constant but varied in the range of $2.5 \times 10^{-5} - 2 \times 10^{-3}$ s^{-1} as the initial GSA concentration varied from 2.8×10^{9} to 2×10^{12} cm^{-3} (Table 2). Two orders of magnitude smaller values for A have been found in the ambient field measurements (e.g. Sihto et al., 2006; Paasonen et al., 2010) and in the laboratory measurements (Sipilä et al., 2010). It should be noted that the exhaust GSA concentrations are much higher than in the atmosphere, and the formation mechanism might be different as well. As seen from Table 2, the modelled total number concentrations (particles > 3 nm) were in good agreement with the measurements.

By using the KIN mechanism the kinetic coefficient K and condensable vapour concentration were varied (Table 2). As an example, Fig. 4 presents the results for 100 % engine load with $K = 5.5 \times 10^{-17}$ cm^3 s^{-1} and COV = 6×10^{11} cm^{-3}. Also with this mechanism nucleation occurred continuously, but the nucleation rate decreased faster than with the ACT mechanism (Fig. S4). The concentrations of particles larger than 3 nm (N_3) and size distributions were in good agreement with the measurements (Table 2). However, sulphuric acid alone was not sufficient to grow the particles to the detectable sizes.

The obtained coefficients A and K vary strongly as a function of the initial GSA concentration. This indicates that nucleation is affected by some other factors than the sulphuric acid concentration. Paasonen et al. (2010) suggested that, besides the organic vapours participate in the initial growth of the nucleated particles, they might also be involved in the nucleation process itself. This idea is supported by the results of the chamber measurements by Dal Maso et al. (2014).

ACPD
15, 4219–4263, 2015

3.1.3 Heteromolecular nucleation

Finally, the fourth set of simulations was performed by assuming homogeneous heteromolecular nucleation between sulphuric acid and organic vapour molecules (adipic acid) along with the homogeneous homomolecular nucleation of sulphuric acid. The coefficients K_1 and K_2 were determined statistically by making a least square fit for the equation

$$K[\mathrm{GSA}]^2 = K_1[\mathrm{GSA}]^2 + K_2[\mathrm{GSA}][\mathrm{COV}] \quad (4)$$

where we assumed that the nucleation rates by the kinetic theory (left-hand side) and by the heteromolecular nucleation theory (right-hand side) were equal. This procedure resulted in constant values of 3.8×10^{-17} and 5.6×10^{-17} cm^3 s^{-1} for K_1 and K_2, respectively, for each of the cases. Hereafter, only these two values are used in the heteromolecular nucleation for each different case. GSA and COV concentrations for the HET nucleation (used in Eq. 4) were the same as for the KIN nucleation in the respective case, i.e. as provided in Table 2. Interestingly, the COV concentration was almost constant, around 1.7×10^{12} cm^{-3}, except for the two lowest GSA cases in which no nucleation occurred, and with the extremely high GSA concentration in which case the particles could notable grow by the GSA. However, the sensitivity of particle number size distribution against the COV concentration will be presented in Sect. 3.3.2.

Although both nucleation and condensation consumed the COV, its high concentration ensured that the size distribution with the initial GSA = 2.0×10^{12} cm^{-3} and COV = 6.0×10^{11} cm^{-3} remained the same as presented for the KIN mechanism where COV was consumed only by condensation (Fig. 4). This case is named hereafter as the base case.

By using the same K_1 and K_2 values for the other initial GSA values (Table 1) the model was able to predict the size distributions which were in good agreement with the experiments. The modal mean diameters of the volatile nucleation mode coincided with the measured ones even though the model predicted stronger NUP formation than

ACPD
15, 4219–4263, 2015

measured if the GSA concentration exceeded 10^{11} cm^{-3} (Fig. 5b). In regard to the non-volatile core mode the model overestimated the growth of particles and slightly underestimated their number concentration. The reason might be too high water content of these non-volatile particles in the model. On the other hand, the SMPS measured mobility diameters which do not grow in spite of substantial condensation occurs if the particles are fractal-like as soot particles. We cannot exclude the possibility of fractal structure of core particles, or condensation of other organic vapours.

The MAFOR model with somewhat different organic condensation processes predicted well the GMDs and number concentrations in the base case but underestimated the NUP concentrations at GSA below 1×10^{11} cm^{-3}. Hygroscopic properties of COV in MAFOR are that of sodium succinate (Peng and Chan, 2001) with a growth factor of 1.85 at RH > 48 %, similar to ammonium sulphate ($(NH_4)_2SO_4$) but somewhat lower than pure H_2SO_4. However, the particle distribution in MAFOR is initially non-hygroscopic (non-volatile core and soot particles) and becomes increasingly hygroscopic through condensation of GSA and COV. An additional non-hygroscopic condensing organic vapour ELVOC with saturation vapour pressure of $C_{34}H_{17}$ (p^0 (298 K) $= 5.0 \times 10^{-11}$ Pa, Lemmon and Goodwin, 2000) was added in the MAFOR simulations to compensate for the initially lower hygroscopic growth and to promote NUP growth to measured size.

3.2 Mass size distribution

As mentioned above additional model simulations for the base case (raw exhaust GSA $= 2 \times 10^{12}$ cm^{-3}) were carried out by the MAFOR model. With MAFOR it is possible to track the mass composition of each size bin during the simulation. Figure 6 shows the time development of the number size distribution and Fig. 7 the mass and composition size distributions. The initial raw exhaust particle distribution at $t = 0.0$ s was assumed to be entirely non-hygroscopic. It was divided into the core mode be-

ACPD
15, 4219–4263, 2015

tween 5–15 nm consisting of non-volatile organic matter (NV POM) and the soot mode consisting of elemental carbon.

During the dilution stage, rapid nucleation of GSA and COV occurred to form a new volatile particle mode with GMD at ∼ 2 nm at 0.1 s (red lines in Fig. 6). By condensation of sulphuric and adipic acids the exhaust particles became more hygroscopic. The growth of the volatile particle mode was promoted by condensation of ELVOC in the MAFOR simulation. Core mode composition at 0.1 s (mass fraction in percentage) was 4.5 % NV POM, 18.9 % sulphuric acid, 2.1 % semi-volatile organic matter (SV OM), 32.2 % extremely low-volatile organic matter (ELV OM), and 41.3 % water. In the ageing chamber, the volatile and core particle modes grew further by condensation of GSA, COV, ELVOC and water. Nucleation by the HET mechanism continuously produced new particles which were scavenged or grown to larger particles. Total particle mass increased from 3.5 $\mu g\,m^{-3}$ at 0.1 s to 28.2 $\mu g\,m^{-3}$ at 0.9 s, and further to 116.8 $\mu g\,m^{-3}$ after 2.7 s. At 0.9 s GMD of volatile mode and core mode increased to 8–9 nm and ∼ 20 nm, respectively. The percentage mass fraction of condensed organic matter increased to 55.5 % while that of water and sulphuric acid decreased to 29.9 and 13.7 %, respectively.

At the end of the simulation (2.7 s) the measured GMD of volatile and core mode was 13.1 and 24.7 nm, respectively, closely matched by the models. Both models underestimated particle number concentrations of the core mode. The modelled mass fractions of the final exhaust particle composition are given in Table 3. According to MAFOR, the final mode of particles with a non-volatile core consisted of 78.0 % condensed organic matter, 6.8 % sulphuric acid and 15.0 % water. Initially present non-volatile organic particles formed the nuclei for condensation of gas-phase vapours in the core mode. However, NV POM contributed negligible to the final mass of the core mode. MAFOR probably underestimated the water content of the exhaust particles by assuming that ELVOC was non-hygroscopic.

ACPD
15, 4219–4263, 2015

3.3 Sensitivity analysis

The sensitivity of particle number size distribution against the dilution time constant, condensable organic vapour concentration, and engine load was tested by AEROFOR for the base case.

3.3.1 Effects of dilution time constant

After 0.1 s the exhaust enters into the ageing chamber. If the dilution time constant τ_d increases from 0.12 s (base case) to e.g. 0.5 s, dilution of exhaust gases continues further in the ageing chamber than for the base case. It should be noted that dilution only occurs when the simulation time is less than τ_d. Due to slower momentary dilution rate the gas concentrations are at first higher leading to stronger nucleation and new particle formation (Fig. 8). However, simultaneously the condensation sink by pre-existing and nucleated particles grows consuming both gases more efficiently, and after 0.4 s from the beginning the gas concentrations and nucleation rate become lower than those of the base case. After that the growth rate of particle number concentration depletes and stabilizes to somewhat smaller number as in the base case. Figure 8c shows that in general, the modal sizes of the final distribution are rather close to that of the base case but their concentrations are lower.

When the time constant decreases to 0.075 s, all dilution occurs before the exhaust enters into the ageing chamber. This leads to very fast reduction of the gas concentrations, and subsequently decreases nucleation and total condensation. Therefore, the final gas concentrations remain higher unlike the particle concentration and their sizes that are smaller than in the base case. The laboratory studies by Mathis et al. (2005) showed that dilution conditions such as dilution ratio, temperature and relative humidity of the dilution air strongly affect the formation of volatile nucleation mode.

ACPD
15, 4219–4263, 2015

3.3.2 Effects of condensable organic vapour

Figure 9 illustrates the number size distribution as a function of COV concentration. As expected, an increase in COV concentration increases nucleation rate and new particle production. Simultaneously, the enhanced condensation of GSA and COV consumes these vapours, and after 1.2 s nucleation dramatically drops, particle number concentration stabilizes, but particles still continue growing to larger sizes. All in all, the final nucleation mode accounts for too many particles, around 3-fold compared with the base case, besides this mode has grown so much that it totally covers the core mode. In fact, the geometric mean diameter of the mode was doubled up to 25 nm. The situation is vice versa, if the COV concentrations is decreased. The nucleated particle concentration remains too low and they don't grow sufficiently to reach the measured sizes.

3.3.3 Effects of pre-existing non-volatile particles

The base case simulation was repeated for different concentrations of initial soot and core particles. As mentioned earlier, these non-volatile particles were formed during the combustion process, and engine technology along with combustion optimization, fuel and lubricant oil compositions, after-treatment systems, and engine load affect their formation and concentrations. Lähde et al. (2010) found that while the non-volatile soot mode concentration decreased, the non-volatile nucleation mode concentration increased for a heavy duty diesel engine. In these simulations the initial non-volatile soot mode concentration varied between 1.1×10^6 and 6.8×10^7 cm^{-3}, and the soot mode between 2.6×10^5 and 1.5×10^7 cm^{-3} (Fig. 10a) while the geometric mean diameters and SDs of the modes were kept constant as given by Table 1.

Figure 10b shows the nucleated particle (NUP) concentration at the end of the ageing chamber as a function of condensation sink (CS) of pre-existing soot and core particles. The NUP concentration was manually calculated or if possible, determined by fitting three modes on the final size distribution (Hussein et al., 2005). It is obvi-

ACPD
15, 4219–4263, 2015

ous that while the CS decreases the NUP concentration increases. If CS $\geq 1\,s^{-1}$, the NUP concentrations linearly depends on the logarithm of the CS. This occurs if the initial dry soot mode concentration is larger than $1.0 \times 10^6\,cm^{-3}$ and the core mode concentration larger than $1.5 \times 10^7\,cm^{-3}$. It should be noted that due to small sizes the effect of the core mode on the CS is small indeed. The maximum NUP concentration is $1.7 \times 10^7\,cm^{-3}$ when the CS is zero. This corresponds to cases that vehicles are equipped by modern diesel particle filters (DPF), the efficiency of those in solid particle number reduction is nowadays even 99.9 %. The NUP formation is ceased if the CS is as high as $52\,s^{-1}$. This occurs if the soot mode and core mode concentrations at hot exhaust (696 K) are for example, 6.8×10^7 and $2.6 \times 10^5\,cm^{-3}$, respectively, with the modal sizes as given in Table 1.

These results also indicate that a reduction in non-volatile particle concentrations as a result of modern engines and particle filters actually enhance nucleation and volatile particle emissions as also found by Du and Yu (2006).

3.3.4 Effects of engine load

Driving conditions at 100 and 75 % engine loads had minor effects on the number concentrations of soot mode and core mode particles (Table 1) whereas at 50 % engine load the soot mode concentration was significantly lower and core mode concentration higher than at the higher loads leading to much lower condensation sink of $2.5\,s^{-1}$ (Fig. 10b). Additionally, due to lower temperatures at lower loads the SO_2 to SO_3 conversion in the catalyst is less efficient, and subsequently the GSA concentration remains lower, in the stabilised phase $3 \times 10^{11}\,cm^{-3}$ (Fig. 2). This, in turn, led to lower NUP formation, in maximum $3.4 \times 10^6\,cm^{-3}$ at the end of the simulation. At 50 % engine load no NUP formation was predicted.

ACPD
15, 4219–4263, 2015

3.4 Effect of FSC

The aim of the last set of simulations was to find the initial GSA concentration when nucleation is ceased at 100 % engine load (T = 697 K) for the base case (CS = 3.5 s^{-1}) and for the case when all non-volatile particles were filtered (CS = 0 s^{-1}). The highest GSA value of 2×10^{12} cm^{-3} was reached when the engine was operated by diesel with the FSC of 36 ppm (Fig. 11). It should be noted that the GSA concentration depends also on the sulphur content of the lubricant oil. If the DPF was used the NUP concentration was 1.9×10^{7} cm^{-3}, two times higher than that if the cDPF was used. In both cases, the NUP concentrations decreased with lower GSA concentrations, and ceased when the GSA concentration was around 10^{10} cm^{-3}. This value corresponds to the fuel with FSC < 1 ppm (Arnold et al., 2012). On the other hand, the GSA concentration of 3×10^{11} cm^{-3} was measured by Arnold et al. (2012) when the FSC was 6 ppm. As seen from Fig. 11, the NUP formation does not depend linearly on the GSA concentration. For example, by decreasing the GSA concentration by 85 % from 2×10^{12} to 3×10^{11} cm^{-3} the NUP concentrations decreases only 15–25 %.

4 Concluding remarks

Although our model simulations cover the exhaust particle formation and growth during the laboratory sampling, the results might be generalized to concern the atmospheric conditions as well. It is well-known that nucleation mode formation at the laboratory tests is very sensitive to the dilution conditions (Khalek et al., 2003; Mathis et al., 2004). However, our on-road and laboratory measurements (Rönkkö et al., 2006, 2007) showed that the volatile nucleation mode was already formed in the atmosphere in less than 0.7 s, at closer than 10 m distance from the exhaust pipe, and that the dilution system along with the ageing chamber used in these measurements mimics reasonably well the real-world conditions and size distributions measured on-road. The exhaust

ACPD
15, 4219–4263, 2015

plume age of 0.4–0.7 s in the atmosphere corresponds to the atmospheric dilution ratio of around 200–400 (Kittelson et al., 1998).

The aerosol dynamics models used in this work are process models that describe the main aerosol processes in details. They use sectional representations for particle size distributions with 100 size sections to prevent numerical diffusion and are free from assumptions of lognormal particle modes that are used in modal models. Several nucleation mechanisms and their potential to predict particle formation in diesel exhaust were investigated. The best fit with the measurements was predicted by the HET nucleation mechanism in which both sulphuric acid and low-volatile organic acid (proxy, adipic acid) molecules participate. Nucleation was occurring continuously in the ageing chamber producing stable clusters of the 1.5 nm size. Due to the competition of coagulation and condensation these freshly formed particles were scavenged or grew to larger sizes. The nucleation rate decreased as a function of elapsed time due to the increased condensation sink and subsequent reduction of the nucleating vapours. However, at the end of the simulation the model predicted 2.8×10^5 particles per cm^3 in the size range of 1.5–3 nm at 100 % engine load, and 3.0×10^5 cm^{-3} at 75 % engine load. These results suggest a hypothesis that diesel exhaust might yield a reservoir of small clusters that activate to grow to even CCN sizes if sufficient amounts of condensable vapours are present.

According to the model simulations the proxy, adipic acid, accounted for the growth since GSA alone was not sufficient. MAFOR predicted that the aged exhaust particles contained 9–10 % adipic acid and 6–7 % sulphuric acid in terms of mass. The required adipic acid concentrations in both models were as high as $(0.6 - 1.8) \times 10^{12}$ cm^{-3} in the raw exhaust. If so, the modern DOC does not prevent totally formation of organic condensable vapours. The adipic acid concentration at the end of the simulation was around 1.1×10^{11} cm^{-3} at 100 % engine load and 6.5×10^{10} cm^{-3} at 75 % engine load. This indicates that diesel exhaust also emits precursor vapours for secondary organic aerosol as recently reported by Robinson et al. (2007).

ACPD
15, 4219–4263, 2015

Despite the known health and climate effects of particle emissions the volatile nucleation mode particles emitted from diesel engines are not regulated. To fulfill the Euro 6 standards new diesel vehicles have to be equipped by DPFs which remove core and soot mode particles. However, based on the model simulations the NUP concentration at high load can be 1.7×10^7 cm^{-3} if the raw exhaust GSA concentration was 2×10^{12} cm^{-3}. The GSA concentration depends besides on the sulphur content of the fuel and the lubricant oil also on driving history. Decreasing the FSC from 36 to 6 ppm the GSA concentration decreased 85 % from 2×10^{12} to 3×10^{11} cm^{-3}, and the subsequent decrease in the NUP concentrations was 15–25 %. The NUP formation was in practice suppressed if the GSA concentration was below 10^{10} cm^{-3}. This requires the use of biodiesel. Also the development of lubricant oil additives might reduce their sulphur content and subsequent particle emissions.

The Supplement related to this article is available online at doi:10.5194/acpd-15-4219-2015-supplement.

Acknowledgements. This work was a part of the TREAM-project and supported by the Finnish Funding Agency for Technology and Innovation (TEKES), AGCO Power, Neste Oil, Dinex Ecocat and Oy Nanol Technologies Ab.

References

Albriet, B., Sartelet, K. N., Lacour, S., Carissimo, B., and Seigneur, C.: Modelling aerosol number distributions from a vehicle exhaust with an aerosol CFD model, Atmos. Environ., 44, 1126–1137, 2010.

Alföldy, B., Gieschaskiel, B., Hofmann, W., and Drossinos, Y.: Size-distribution dependent lung deposition of diesel exhaust particles, J. Aerosol Sci., 40, 652–663, 2009.

Almeida, J., Schobesberger, S., Kürten, A., Ortega, I. K., Kupiainen-Määttä, O., Praplan, A. P., Adamov, A., Amorim, A., Bianchi, F., Breitenlechner, M., David, A., Dommen, J., Donahue, N.

ACPD
15, 4219–4263, 2015

M., Downard, A., Dunne, E., Duplissy, J., Ehrhart, S., Flagan, R. C., Franchin, A., Guida, R., Hakala, J., Hansel, A., Heinritzi, M., Henschel, H., Jokinen T., Junninen, H., Kajos, M., Kangasluoma, J., Keskinen, H., Kupc, A., Kurtén, T., Kvashin, A. N., Laaksonen, A., Lehtipalo, K., Leiminger, M., Leppä, J., Loukonen, V., Makhmutov, V., Mathot, S., McGrath, M. J., Nieminen, T., Olenius, T., Onnela, A., Petäjä, T., Riccobono, F., Riipinen, I., Rissanen, M., Rondo, L., Ruuskanen, T., Santos, F. D., Sarnela, N., Schallhart, S., Schnitzhofer, R., Seinfeld, J. H., Simon, M., Sipilä, M., Stozhkow, Y., Stratmann, F., Tomá, A., Tröstl, J., Tsagkogeorgas, G., Vaattovaara, P., Viisanen, Y., Virtanen, A., Vrtala, A., Wagner, P. E., Weingartner, E., Wek, H., Willamson, C., Wimeer, D., Ye, P., Yli-Juuti, T., Carslaw, K. S., Kulmala, M., Curtius, J., Baltenspenger, U., Worsnop, D. R., Vehkamäki, H., and Kirkby, J.: Molecular understanding of sulphuric acid-amine particle nucleation in the atmosphere, Nature, 502, 359–363, doi:10.1038/nature12663, 2013.

Arnold, F., Curtius J., Sierau, B., Bürger, V., Busen, R., and Schumann, U.: Detection of massive negative chemiions in the exhaust plume of a jet aircraft in flight, Geophys. Res. Lett., 26, 1577–1580, 1999.

Arnold, F., Pirjola, L., Aufmhoff, H., Schuck, T., Lähde, T., and Hämeri, K.: First gaseous sulfuric acid measurements in automobile exhaust: implications for volatile nanoparticle formation, Atmos. Environ., 40, 7097–7105, 2006.

Arnold, F., Pirjola, L., Rönkkö, T., Reichl, U., Schlager, H., Lähde, T., Heikkilä, and J., Keskinen, J.: First on-line measurements of sulphuric acid gas in modern heavy duty diesel engine exhaust: implications for nanoparticle formation, Environ. Sci. Technol., 46, 11227–11234, 2012.

Bilde, M., Svenningsson, B., Mønster, J., and Rosenørn, T.: Even-odd alternation of evaporation rates and vapor pressures of C3–C9 dicarboxylic acid aerosols, Environ. Sci. Technol., 37, 1371–1378, 2003.

Bond, T. C., Doherty, S. J., Fahey, D. W., Forster, P. M., Berntsen, T., DeAngelo, B. J., Flanner, M. G., Ghan, S., Kärcher, B., Koch, D., Kinne, S., Kondo, Y., Quinn, P. K., Sarofim, M. C., Schultz, M. G., Schultz, M., Venkataraman, C., Zhang, H., Zhang, S., Bellouin, N., Guttikunda, S. K., Hopke, P. K., Jacobson, M. Z., Kaiser, J. W., Klimont, Z., Lohmann, U., Schwarz, J. P., Shindell, D., Storelvmo, T., Warren, S. G., and Zender, C. S. Bounding the role of black carbon in the climate system: a scientific assessment, J. Geophys. Res. Atmos., 118, 5380–5552, 2013.

ACPD
15, 4219–4263, 2015

Charlson, R. J., Schwartz, S. E., Hales, J. M., Cess, R. D., Coakley, J. A., Hansen, J. E., and Hofmann, D. J.: Climate forcing by anthropogenic aerosols, Science, 255, 423–430, 1992.
Dal Maso, M., Liao, L., Wildt, J., Kiendler-Scharr, A., Kleist, E., Tillmann, R., Sipilä, M., Hakala, J., Lehtipalo, K., Ehn, M., Kerminen, V.-M., Kulmala, M., Worsnop, D., and Mentel, T.: A chamber study of the influence of boreal BVOC emissions and sulphuric acid on nanoparticle formation rates at ambient concentrations, Atmos. Chem. Phys. Discuss., 14, 31319-31360, doi:10.5194/acpd-14-31319-2014, 2014.
Du, H. and Yu, F.: Role of the binary H_2SO_4-H_2O homogeneous nucleation in the formation of volatile nanoparticles in the vehicular exhaust, Atmos. Environ., 40, 7579–7588, 2006.
Du, H. and Yu, F.: Nanoparticle formation in the exhaust of vehicles running on ultra-low sulfur fuel, Atmos. Chem. Phys., 8, 4729–4739, doi:10.5194/acp-8-4729-2008, 2008.
Fiedler, V., Dal Maso, M., Boy, M., Aufmhoff, H., Hoffmann, J., Schuck, T., Birmili, W., Hanke, M., Uecker, J., Arnold, F., and Kulmala, M.: The contribution of sulphuric acid to atmospheric particle formation and growth: a comparison between boundary layers in Northern and Central Europe, Atmos. Chem. Phys., 5, 1773–1785, doi:10.5194/acp-5-1773-2005, 2005.
Filippo, A. and Maricq, M.: Diesel nucleation mode particles: semivolatile or solid?, Environ. Sci. Technol., 42, 7957–7962, 2008.
Fuchs, N. A.: The Mechanics of Aerosols, transl by: Daisley, R. E. and Fuchs, M., Dover Publications, New York, 1964.
Fuchs, N. A. and Sutugin, A. G.: High dispersed aerosols, in: Topics in Current Aerosol Research (Part 2), edited by: Hidy, G. M. and Brock, J. R., Pergamon, New York, 1971.
Numerical Algorithms Group: The NAG Workstation Library Handbook 1. FORTRAN-routine DO2EJF: The NAG Workstation Library Handbook 1. The Numerical Algorithms Group Ltd., Oxford, 1990.
Giechaskiel, B., Ntziachristos, L., Samaras, Z., Scheer, V., Casati, R., and Vogt, R.: Formation potential of vehicle exhaust nucleation mode particles on-road and in the laboratory, Atmos. Environ., 39, 3191–3198, 2005.
Giechaskiel, B., Ntziachristo, L., and Samaras, Z.: Effect of ejector dilutors on measurements of automotive exhaust gas aerosol size distributions, Meas. Sci. Technol., 20, 45703–45710, 2009.
Hämeri, K., Charlson, R., and Hansson, H.-C., Hygroscopic properties of mixed ammonium sulfate and carboxylic acid particles, AIChE J., 48, 1309–1316, 2002.

ACPD
15, 4219–4263, 2015

Heikkilä, J., Rönkkö, T., Lähde, T., Lemmetty, M., Arffman, A., Virtanen, A., Keskinen, J., Pirjola, L., and Rothe, D.: Effect of open channel filter on particle emissions of modern diesel engine, J. Air Waste Manage., 59, 1148–1154, doi:10.3155/1047-3289.59.10.1148, 2009.

Hussein, T., Dal Maso, M., Petäjä, T., Koponen, I. K., Paatero, P., Aalto, P. P., Hämeri, K., and Kulmala, M.: Evaluation of an automatic algorithm for fitting the particle number size distributions, Boreal Environ. Res., 10, 337–355, 2005.

Jacobson, M. Z.: Numerical techniques to solve condensational and dissolutional growth equations when growth is coupled to reversible reactions, Aerosol Sci. Technol., 27, 491–498, 1997.

Karjalainen, P., Pirjola, L., Heikkilä, J., Lähde, T., Tzamkiozis, T., Ntziachristos, L., Keskinen, J., and Rönkkö, T.: Exhaust particles of modern gasoline vehicles: laboratory and on-road study, Atmos. Environ., 97, 262–270, 2014.

Karl, M., Gross, A., Pirjola, L., and Leck, C.: A new flexible multicomponent model for the study of aerosol dynamics in the marine boundary layer, Tellus B, 63, 1001–1025, doi:10.1111/j.1600-0889.2011.00562.x, 2011.

Karl, M., Leck, C., Gross, A., and Pirjola, L.: A study of new particle formation in the marine boundary layer over the central Arctic Ocean using a flexible multicomponent aerosol dynamic model, Tellus B, 64, 17158, doi:10.3402/tellusb.v64i0.17158, 2012a.

Karl, M., Dye, C., Schmidbauer, N., Wisthaler, A., Mikoviny, T., D'Anna, B., Müller, M., Borrás, E., Clemente, E., Muñoz, A., Porras, R., Ródenas, M., Vázquez, M., and Brauers, T.: Study of OH-initiated degradation of 2-aminoethanol, Atmos. Chem. Phys., 12, 1881–1901, doi:10.5194/acp-12-1881-2012, 2012b.

Keskinen, J., Pietarinen, K., and Lehtimäki, M.: Electrical low pressure impactor, J. Aerosol Sci., 23, 353–360, 1992.

Kettunen, J., Lanki, T., Tiittanen, P., Aalto, P. P., Koskentalo, T., Kulmala, M., Salomaa, V., and Pekkanen, J.: Associations of fine and ultrafine particulate air pollution with stroke mortality in an area of low air pollution levels, Stroke, 38, 918–922, 2007.

Keuken, M. P., Henzing, J. S., Zandveld, P., van den Elshout, S., and Karl, M.: Dispersion of particle numbers and elemental carbon from road- traffic, a harbor and an airstrip in the Netherlands, Atmos. Environ., 54, 320–327, 2012.

Khalek, I. A., Spears, M., and Charmley, W.; Particle size distribution from heady-duty diesel engine: steady-state and transient emission measurement using two dilution systems and two fuels, SAE Technical Paper Series, 2003-01-0285, 2003.

ACPD
15, 4219–4263, 2015

Kittelson, D. B.: Engines and nanoparticles: a review, J. Aerosol Sci., 29, 575–588, 1998.
Kittelson, D. B., Watts, W. F., Johnson, J. P., Thorne, C., Higham, C., Payne, J., Goodier, S., Warrens, C., Preston, H., Zink, U., Pickles, D., Goersmann, C., Twigg, M. V., Walker, A. P., and Boddy, R.: Effect of fuel and lube oil sulfur on the performance of a diesel exhaust gas continuously regenerating trap. Environ. Sci. Technol, 42, 9276–9282, 2008.
Kulmala, M., Laaksonen, A., and Pirjola, L.: Parameterizations for sulfuric acid/water nucleation rates, J. Geophys. Res., 103, 8301–8308, 1998.
Kulmala, M., Dal Maso, M., Mäkelä, J. M., Pirjola, L., Väkevä, M., Aalto, P., Miikkulainen, P., Hämeri, K., and O'Dowd, C. D.: On the formation, growth and composition of nucleation mode particles, Tellus B, 53, 479–490, 2001.
Kulmala, M., Lehtinen, K. E. J., and Laaksonen, A.: Cluster activation theory as an explanation of the linear dependence between formation rate of 3nm particles and sulphuric acid concentration, Atmos. Chem. Phys., 6, 787–793, doi:10.5194/acp-6-787-2006, 2006.
Kulmala, M., Riipinen, I., Sipilä, M., Manninen, H. E., Petäjä, T., Junninen, H., Dal Maso, M., Mordas, G., Mirme, A., Vana, M., Hirsikko, A., Laakso, L., Harrison, R. M., Hanson, I., Leung, C., Lehtinen, K. E. J., and Kerminen, V-M.:: Toward direct measurement of atmospheric nucleation, Science, 318, 89–92, 2007.
Lähde, T., Rönkkö, T., Virtanen, A., Solla, A., Kytö, M., Söderström, C., and Keskinen, J.: Dependence between non-volatile nucleation mode particle and soot number concentrations in an EGR equipped heavy duty diesel engine exhaust, Environ. Sci. Technol., 44, 3175–3180, 2010.
Lehtinen, K. E. J. and Kulmala, M.: A model for particle formation and growth in the atmosphere with molecular resolution in size, Atmos. Chem. Phys., 3, 251–257, doi:10.5194/acp-3-251-2003, 2003.
Lemmon, E. W. and Goodwin, A. R. H.: Critical properties and vapor pressure equation for alkanes C_nH_{2n+2}: normal alkanes and isomers for $n = 4$ through $n = 9$, J. Phys. Chem. Ref. Data, 29, 1–39, 2000.
Lemmetty, M., Pirjola, L., Mäkelä, J. M., Rönkkö, T., and Keskinen, J.: Computation of maximum rate of water–sulphuric acid nucleation in diesel exhaust, J. Aerosol Sci., 37, 1596–1604, 2006.
Lemmetty, M., Rönkkö, T., Virtanen, A., Keskinen, J., and Pirjola, L.: The effect of sulphur in diesel exhaust aerosol: models comparison with measurements, Aerosol Sci. Technol., 42, 916–929, doi:10.1080/02786820802360682, 2008.

ACPD
15, 4219–4263, 2015

Liu, Y. H., He, Z., and Chan, T. L.: Three-dimensional simulation of exhaust particle dispersion and concentration fields in the near-wake region of the studied ground vehicle, Aerosol Sci. Technol., 45, 1019–1030, doi:10.1080/02786826.2011.580021, 2011.

Ma, H., Jung, H., and Kittelson, D. B.: Investigation of diesel nanoparticle nucleation mechanism, Aerosol Sci. Technol., 42, 335–342, 2008.

Marick, M., Chase, R., Xu, N., and Laing, P.: The effects of the catalytic converter and fuel sulphur level on motor vehicle particulate matter emissions: light duty diesel vehicles, Environ. Sci. Technol., 36, 283–289, 2002.

Mathis, U., Ristimäki, J., Mohr, M., Keskinen, J., Ntziachristos, L., Samaras, Z., Mikkanen, P.: Sampling conditions for the measurement of nucleation mode particles in the exhaust of a diesel vehicle, Aerosol Sci. Technol., 38, 1149–1160, 2004.

McMurry, P. H. and Friedlander, S. K.: New particle formation in the presence of an aerosol, Atmos. Environ., 13, 1635–1651, 1979.

Merikanto, J., Napari, I., Vehkamäki, H., Anttila, T., and Kulmala, M.: New parameterization of sulfuric acid-ammonia-water ternary nucleation rates at tropospheric conditions, J. Geophys. Res., 112, D15207, doi:10.1029/2006JD007977, 2007.

Napari, I., Noppel, M., Vehkamäki, H., and Kulmala, M.: Parameterization of ternary nucleation rates for H_2SO_4-NH_3-H_2O vapors, J. Geophys. Res., 107, 4381, doi:10.1029/2002JD002131, 2007.

Ntziachristos, L., Giechaskiel, B., Pistikopoulos, P., Samaras, Z., Mathis, U., Mohr, M., Ristimäki, J., Keskinen, J., Mikkanen, P., Casati, R., and Scheer, V., Vogt, R.: Performance evaluation of a novel sampling and measurement system for exhaust particle characterization, SAE Technical Paper Series 2004-01-1439, 2004.

Olin, M., Rönkkö, T., and Dal Maso, M.: CFD modeling of a vehicle exhaust laboratory sampling system: sulfur driven nucleation and growth in diluting diesel exhaust, Atmos. Chem. Phys. Discuss., 15, 2905–2956, doi:10.5194/acpd-15-2905-2015, 2015.

Paasonen, P., Nieminen, T., Asmi, E., Manninen, H. E., Petäjä, T., Plass-Dülmer, C., Flentje, H., Birmili, W., Wiedensohler, A., Hõrrak, U., Metzger, A., Hamed, A., Laaksonen, A., Facchini, M. C., Kerminen, V.-M., and Kulmala, M.: On the roles of sulphuric acid and low-volatility organic vapours in the initial steps of atmospheric new particle formation, Atmos. Chem. Phys., 10, 11223–11242, doi:10.5194/acp-10-11223-2010, 2010.

Peng, C. and Chan, C. K.: The water cycles of water-soluble organic salts of atmospheric importance, Atmos. Environ., 35, 1183–1192, 2001.

ACPD
15, 4219–4263, 2015

Pirjola, L.: Effects of the increased UV radiation and biogenic VOC emissions on ultrafine aerosol formation, J. Aerosol Sci., 30, 355–367, 1999.
Pirjola, L. and Kulmala, M.: Development of particle size and composition distribution with a novel aerosol dynamics model, Tellus B, 53, 491–509, 2001.
Pirjola, L., Lehtinen, K. E. J., Hansson, H.-C., and Kulmala, M.: How important is nucleation in regional/global modelling, Geophys. Res. Lett., 31, L12109, doi:10.1029/2004GL019525, 2004.
Pope III, C. A. and Dockery, D. W.: Health effects of fine particulate air pollution: lines that connect, J. Air Waste Manage., 56, 707–742, 2006.
Pyykönen, J., Miettinen, M., Sippula, O., Leskinen, A., Raunemaa, T., and Jokiniemi, J.: Nucleation in a perforated tube diluter, J. Aerosol Sci., 38, 172–191, 2007.
Raes, F. and Janssens, A.: Ion-induced aerosol formation in a H_2O-H_2SO_4 system. 1. Extension of the classical theory and search for experimental evidence, J. Aerosol Sci., 16, 217–227, 1985.
Robinson, A. L., Donahue, N. M., Shrivastava, M. K., Weitkamp, E. A., Sage, A. M., Grieshop, A. P., Lane, T. E., Pierce, J. R., and Pandis, S. N.: Rethinking organic aerosols: semivolatile emissions and photochemical aging, Science, 315, 1259–1262, 2007.
Rönkkö, T., Virtanen, A., Vaaraslahti, K., Keskinen, J., Pirjola, L., and Lappi, M.: Effect of dilution conditions and driving parameters on nucleation mode particles in diesel exhaust: laboratory and on-road study, Atmos. Environ., 40, 2893–2901, 2006.
Rönkkö, T., Virtanen, A., Kannosto, J., Keskinen, J., Lappi, M., and Pirjola, L.: Nucleation mode particles with a non-volatile core in the exhaust of a heavy duty diesel vehicle, Environ. Sci. Technol., 41, 6384–6389, doi:10.1021/es0705339, 2007.
Rönkkö, T., Lähde, T., Heikkilä, J., Pirjola, L., Bauschke, U., Arnold, F., Schlager, H., Rothe, D., Yli-Ojanperä, J., and Keskinen, J.: Effect of gaseous sulphuric acid on diesel exhaust nanoparticle formation and characteristics, Environ. Sci. Technol., 47, 11882–11889, doi:10.1021/es402354y, 2013.
Schneider, J., Hock, N., Weimer, S., Borrmann, S., Kirchner, U., Vogt, R., and Scheer, V.: Nucleation particles in diesel exhaust: composition inferred from in situ mass spectrometer analysis, Environ. Sci. Technol., 39, 6153–6161, 2005.
Shi, J. and Harrison, R.: Investigation of ultrafine particle formation during diesel exhaust dilution, Environ. Sci. Technol., 33, 3730–3736, 1999.

ACPD
15, 4219–4263, 2015

Sihto, S.-L., Kulmala, M., Kerminen, V.-M., Dal Maso, M., Petäjä, T., Riipinen, I., Korhonen, H., Arnold, F., Janson, R., Boy, M., Laaksonen, A., and Lehtinen, K. E. J.: Atmospheric sulphuric acid and aerosol formation: implications from atmospheric measurements for nucleation and early growth mechanisms, Atmos. Chem. Phys., 6, 4079–4091, doi:10.5194/acp-6-4079-2006, 2006.

Sioutas, C., Delfino, R. J., and Singh, M.: Exposure assessment for atmospheric ultrafine particles (UFPs) and implications in epidemiologic research, Environ. Health Persp., 113, 947–955, 2005.

Sipilä, M., Bernt, T., Petäjä, T., Brus, D., Vanhanen, J., Stratmann, F., Patokoski, J., Mauldin III, R. L., Hyvärinen, A.-P., Lihavainen, H., and Kulmala, M.: The role of sulfuric acid in atmospheric nucleation, Science, 327, 1243, 2010.

Speidel, M., Nau, R., Arnold, F., Schlager, H., and Stohl, A.: Sulfur dioxide measurements in the lower, middle and upper troposphere: deployment of an aircraft-based chemical ionization mass spectrometer with permanent in-flight calibration, Atmos. Environ., 41, 2427–2437, 2007.

Su, D. S., Serafino, A., Müller, J.-O., Jentoft, R. E., Schlögl, R., and Fiorito, S.: Cytotoxicity and inflammatory potential of soot particles of low-emission diesel engines, Environ. Sci. Technol., 42, 1761–1765, 2008.

Tobias, H., Beving, D., Ziemann, P., Sakurai, H., Zuk, M., McMurry, P., Zarling, D., Watylonis, R., and Kittelson, D.: Chemical analysis of diesel engine nanoparticles using a nano-DMA/thermal desorption particle beam mass spectrometer, Environ. Sci. Technol., 35, 2233–2243, 2001.

Uhrner, U., von Löwis, S., Vehkamäki, H., Wehner, B., Bräsel, S., Hermann, M., Stratmann, F., Kulmala, J., and Wiedensohler, A.; Dilution and aerosol dynamics within a diesel car exhaust plume – CFD simulations of on-road measurement conditions, Atmos. Environ., 41, 7440–7461, 2007.

Vaaraslahti, K., Keskinen, J., Giechaskiel, B., Solla, A., Murtonen, T., and Vesala, H.: Effect of lubricant on the formation of heavy-duty diesel exhaust particles, Environ. Sci. Technol., 39, 8497–8504, 2005.

Vehkamäki, H., Kulmala, M., Napari, I., Lehtinen, K. E. J., Timmreck, C., Noppel, M., and Laaksonen, A.: An improved parameterization for sulphuric acid-water nucleation rates for tropospheric and stratospheric conditions, J. Geophys. Res., 107, 4622, doi:10.1029/2002JD002184, 2002.

ACPD
15, 4219–4263, 2015

Vehkamäki, H., Kulmala, M., Lehtinen, K. E. J., Noppel, M.: Modelling binary homogeneous nucleation of water-sulfuric acid vapours: parameterisation for high temperature emissions, Environ. Sci. Technol., 37, 3392–3398, 2003.

Virtanen, A., Ristimäki, J., Marjamäki, M., Vaaraslahti, K., Keskinen, J., and Lappi, M.: Effective density of diesel exhaust particles as a function of size, SAE Tech. Pap. Ser. 2002-01-0056, 2002.

Vouitsis, E., Ntziachristos, L., Samaras, Z.: Modelling of diesel exhaust aerosol during laboratory sampling, Atmos. Environ., 39, 1335–1345, 2005.

Wang, Y. J. and Zhang, W. K. M.: Coupled turbulence and aerosol dynamics modelling of vehicle exhaust plumes using the CTAG model, Atmos. Environ., 59, 284–293, 2012.

Weber, R. J., Marti, J. J., McMurry, P. H., Eisele, F. L., Tanner, D. J., and Jefferson, A.: Measurements of new particle formation and ultrafine particle growth rates at a clean continental site, J. Geophys. Res., 102, 4375–4385, 1997.

Yeung, M. C., Lee, A. K. Y., and Chan, C. K.: Phase transition and hygroscopic properties of internally mixed ammonium sulfate and adipic Acid (AS-AA) particles by optical microscopic imaging and Raman spectroscopy, Aerosol Sci. Technol., 43, 387–399, 2009.

Yu, F. and Turco, R. P.: Ultrafine aerosol formation vie ion-mediated nucleation, Geophys. Res. Lett., 6, 883–886, 2000.

ACPD
15, 4219–4263, 2015

Table 1. Lognormal parameters (number concentration N, geometric mean diameter D_g, SD σ) for non-volatile exhaust particles and GSA concentration in raw exhaust at different engine loads and exhaust temperatures. Index 1 refers to the core mode and index 2 to the soot mode.

Engine load (%)	T (K)	GSA (cm^{-3}) $\times 10^{10}$	N_1 (cm^{-3}) $\times 10^6$	D_{g1} (nm)	σ_1	N_2 (cm^{-3}) $\times 10^6$	D_{g2} (nm)	σ_2
100	697	0.28	1.66	8.8	1.25	1.96	49	2.15
100	697	0.34	1.66	8.8	1.25	1.96	49	2.15
100	697	1.36	1.66	8.8	1.25	1.96	49	2.15
100	697	4.17	1.66	8.8	1.25	1.96	49	2.15
100	697	9.75	1.66	8.8	1.25	1.96	49	2.15
100	697	15.3	1.66	8.8	1.25	1.96	49	2.15
100	697	26.6	1.66	8.8	1.25	1.96	49	2.15
100	697	44.0	1.66	8.8	1.25	1.96	49	2.15
100	697	201	1.66	8.8	1.25	1.96	49	2.15
75	657	11.5	1.53	8.4	1.26	1.79	49	1.98
75	657	25.0	1.53	8.4	1.26	1.79	49	1.98
75	657	30.2	1.53	8.4	1.26	1.79	49	1.98
50	618	11.1	0.427	7.5	1.23	5.34	56	1.87

ACPD
15, 4219–4263, 2015

Table 2. Initial condensable organic vapour concentrations (COV) and activation coefficient (A) as well as the initial COV and kinetic coefficient (K) as a function of the initial gaseous sulphuric acid concentration (GSA). For heterogeneous nucleation GSA, COV and N_{3fin} are as for kinetic nucleation but $K_1 = 3.8 \times 10^{-17}$ and $K_2 = 5.6 \times 10^{-17}$ cm^3 s^{-1} for each case.

Measured	Cluster activation			Kinetic nucleation			Measured
GSA (cm^{-3})	COV (cm^{-3})	A (s^{-1})	N_{3fin} (cm^{-3})	COV (cm^{-3})	K ($cm^3 s^{-1}$)	N_{3fin} (cm^{-3})	N_3 (cm^{-3})
2.76×10^9	6.00×10^{10}	2.00×10^{-3}	6.88×10^5	4.00×10^{10}	1.00×10^{-12}	6.84×10^5	7.69×10^5
3.41×10^9	8.00×10^{10}	2.00×10^{-3}	6.93×10^5	8.00×10^{10}	5.00×10^{-13}	7.52×10^5	1.03×10^6
1.36×10^{10}	1.25×10^{12}	1.00×10^{-3}	3.54×10^6	1.50×10^{12}	5.00×10^{-14}	3.16×10^6	3.13×10^6
4.17×10^{10}	1.50×10^{12}	5.50×10^{-4}	5.97×10^6	1.70×10^{12}	4.00×10^{-15}	5.08×10^6	4.61×10^6
1.53×10^{11}	1.60×10^{12}	2.00×10^{-4}	7.34×10^6	1.70×10^{12}	7.00×10^{-16}	5.79×10^6	5.33×10^6
4.40×10^{11}	1.80×10^{12}	9.00×10^{-5}	9.36×10^6	1.70×10^{12}	2.50×10^{-16}	7.10×10^6	6.57×10^6
2.01×10^{12}	6.00×10^{11}	2.50×10^{-5}	1.14×10^7	6.00×10^{11}	5.50×10^{-17}	9.52×10^6	8.03×10^6

ACPD
15, 4219–4263, 2015

Table 3. Mass fractions of particle components at 2.7 s obtained from simulation by MAFOR with initial GSA = 2×10^{12} cm^{-3}.

	Volatile mode	Core mode	Soot mode
H_2O	0.128	0.150	0.116
H_2SO_4	0.058	0.068	0.053
COV	0.104	0.103	0.092
ELVOC	0.710	0.676	0.531
NVPOM	0.000	0.002	0.000
SOOT	0.000	0.000	0.208
TOT	1.000	1.000	1.000

ACPD
15, 4219–4263, 2015

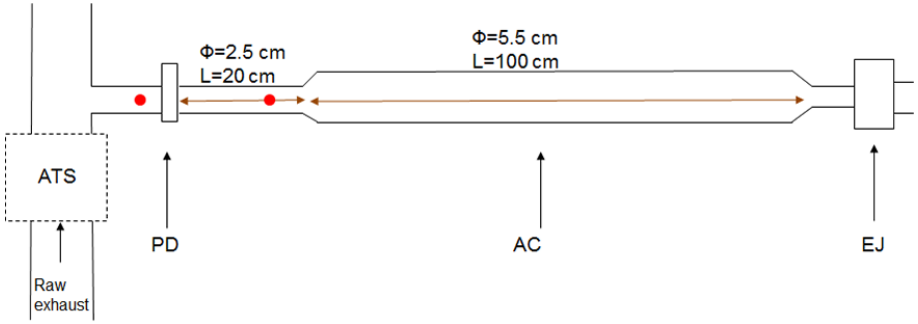

Figure 1. Schematic figure of diluting and ageing exhaust. ATS = after-treatment system, PD = porous diluter (12 : 1), AC = ageing chamber with the volume of 2.4 dm^3, ED = ejector diluter (8 : 1). Red circles refer to temperature measurements. Exhaust flow rate through the dilution/sampling system was kept constant 55 lpm.

ACPD
15, 4219–4263, 2015

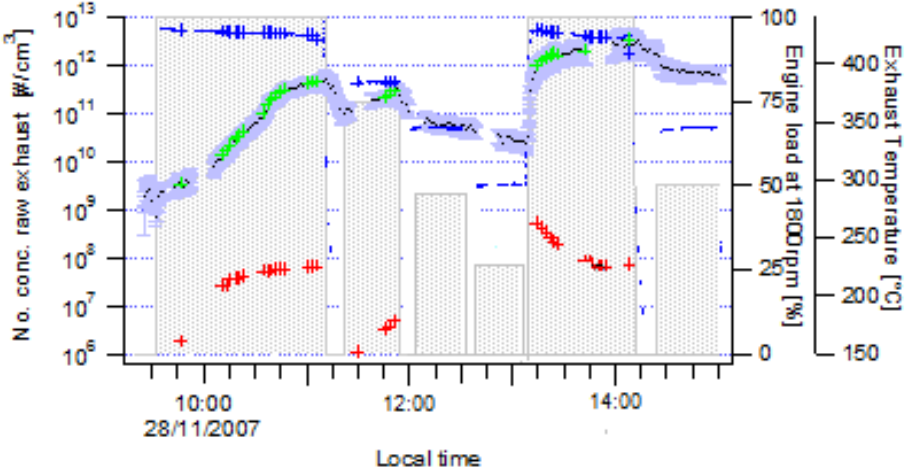

Figure 2. Time series of the concentrations of GSA (blue curve) and particles larger than 3 nm (red crosses) in the raw exhaust as a function of engine load (shaded bars). Also shown is the exhaust temperature (blue crosses).

ACPD
15, 4219–4263, 2015

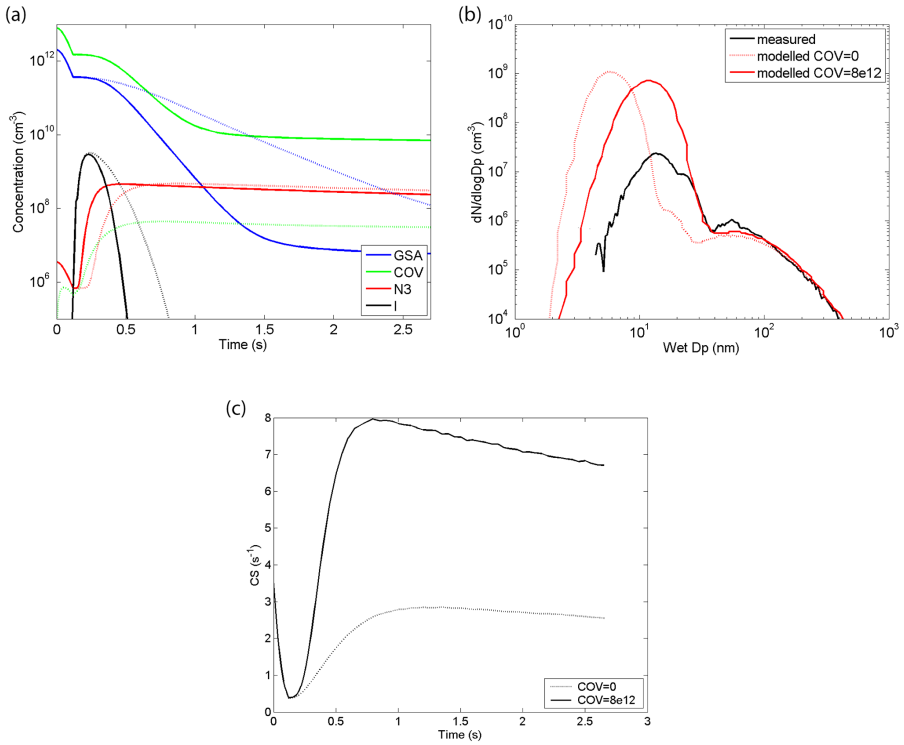

Figure 3. (a) Time evolution of particle number concentration (N_3), gaseous sulphuric acid (GSA) and condensable organic vapour (COV) in cm^{-3}, as well as nucleation rate (J) in cm^{-3} s^{-1} by the BHN mechanism, **(b)** Measured (black) and modelled (red) particle number size distribution at the end of the ageing chamber. **(c)** Condensation sink for sulphuric acid. Initial GSA = 2×10^{12} cm^{-3}, COV = 8×10^{12} cm^{-3} and COV = 0.

ACPD
15, 4219–4263, 2015

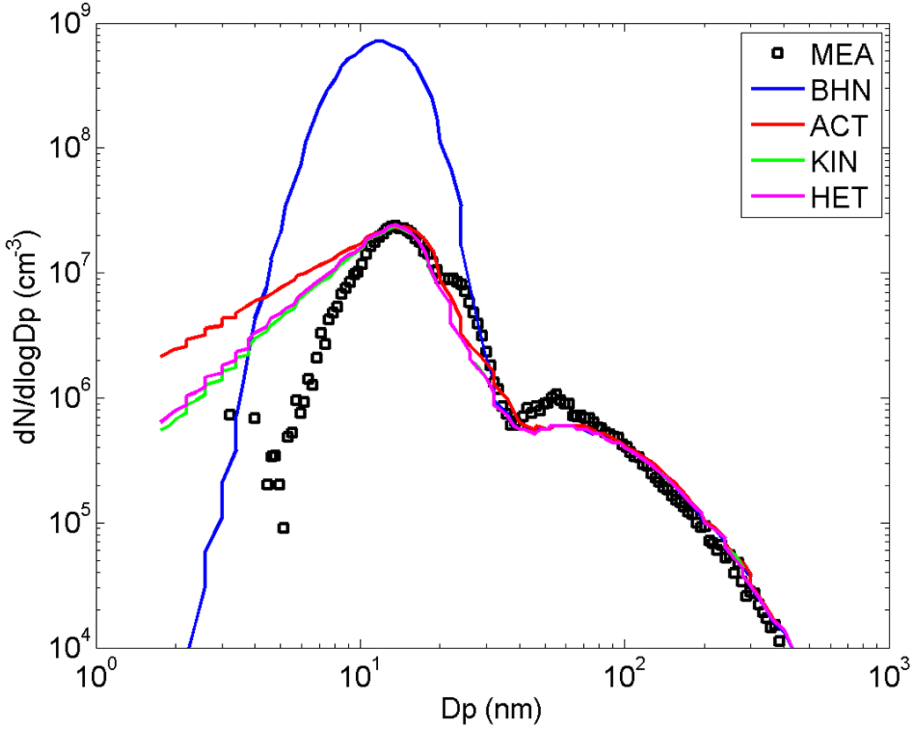

Figure 4. Comparison of measured and modelled particle size distributions, considering different nucleation mechanisms. Engine load was 100 %, initial GSA = 2.0×10^{12} cm^{-3}, COV = 6×10^{11} cm^{-3} except for BHN it was 8×10^{12} cm^{-3}. The simulation time was 2.7 s. Black squares refer to the measured size distribution by the SMPS after the ageing chamber.

ACPD
15, 4219–4263, 2015

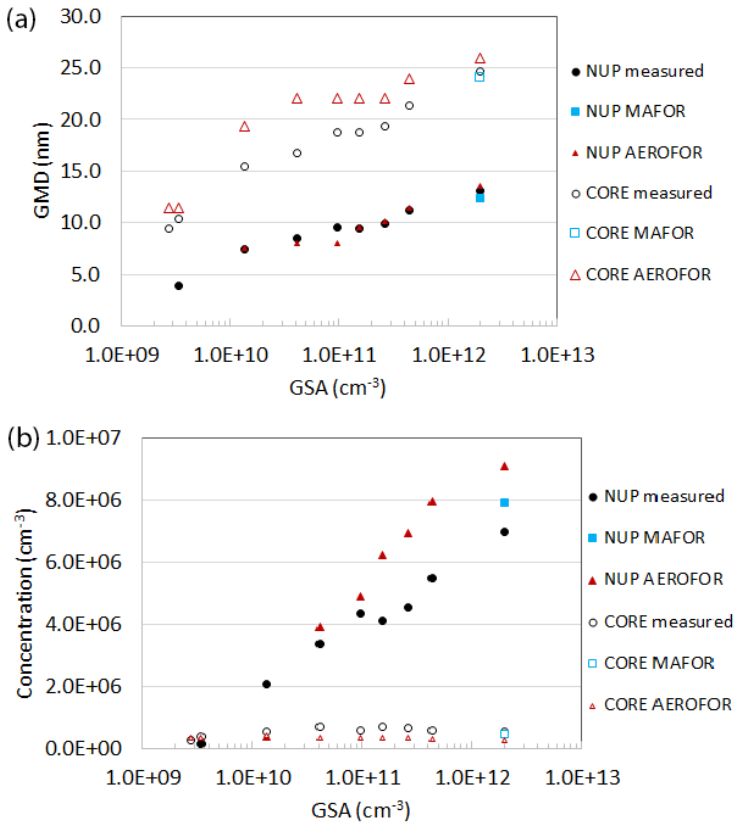

Figure 5. Mean diameters (GMD) **(a)** and number concentration of particles > 3 nm **(b)** at the end of the simulation for the volatile nucleation mode and the non-volatile core mode. Also shown are the measured values at the end of the ageing chamber.

ACPD
15, 4219–4263, 2015

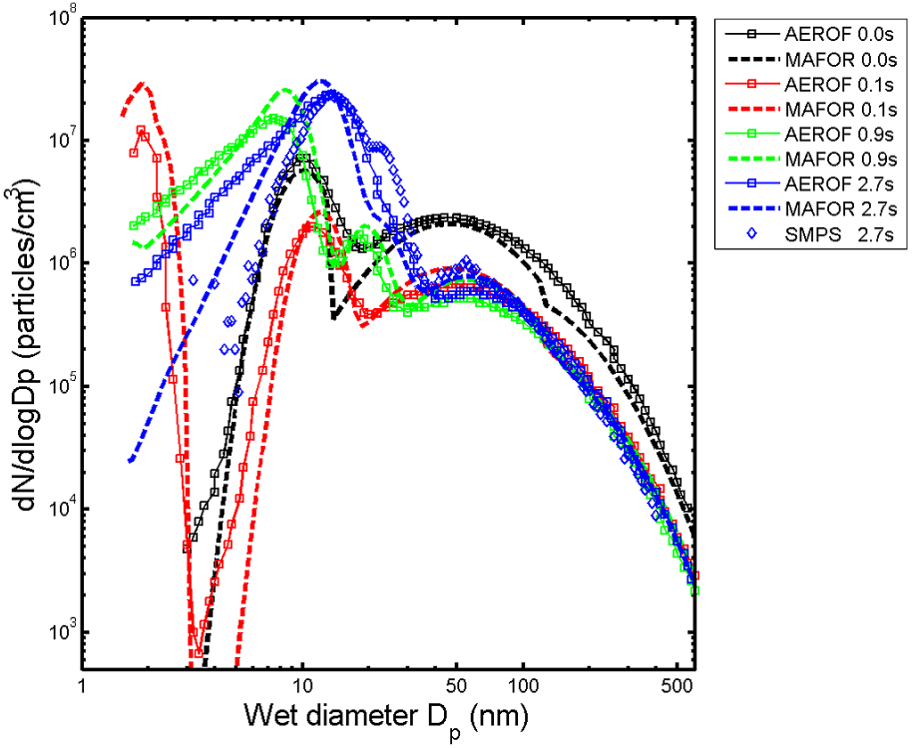

Figure 6. Number size distribution ($dN/d\log D_p$ in particles cm^{-3}) at different stages of the exhaust (t = 0.0 s, black lines; t = 0.1 s, red lines; t = 0.9 s, green lines; t = 2.7 s, blue lines) as modelled by AEROFOR (lines with open squares) and by MAFOR (dashed lines) together with the SMPS measurement at 2.7 s (blue open diamonds). Initial size distribution with the core mode at 10 nm and soot mode at 49 nm.

ACPD
15, 4219–4263, 2015

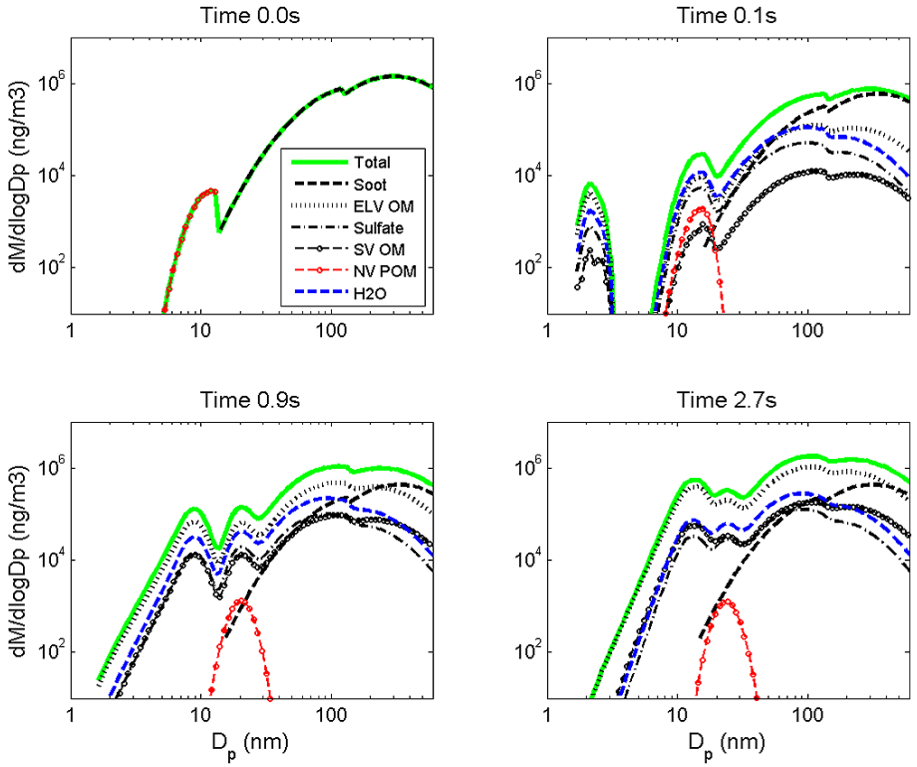

Figure 7. Mass composition distribution ($dM/d\log D_p$ in ng m^{-3}) at different stages of the exhaust (initial at $t = 0.0$ s, after dilution $t = 0.1$ s, in the ageing chamber $t = 0.9$ s, and final $t = 2.7$ s) modelled by MAFOR. Includes the total mass concentration (green line) and the mass distributions of non-volatile organic matter (NV POM, red dashed line with open circles), soot (black dashed line), sulphuric acid (black dash-dotted line), semi-volatile organic matter (SV OM, black dashed line with open circles), extremely low-volatile organic matter (ELV OM) as well as the mass distribution of water (blue dashed line).

ACPD
15, 4219–4263, 2015

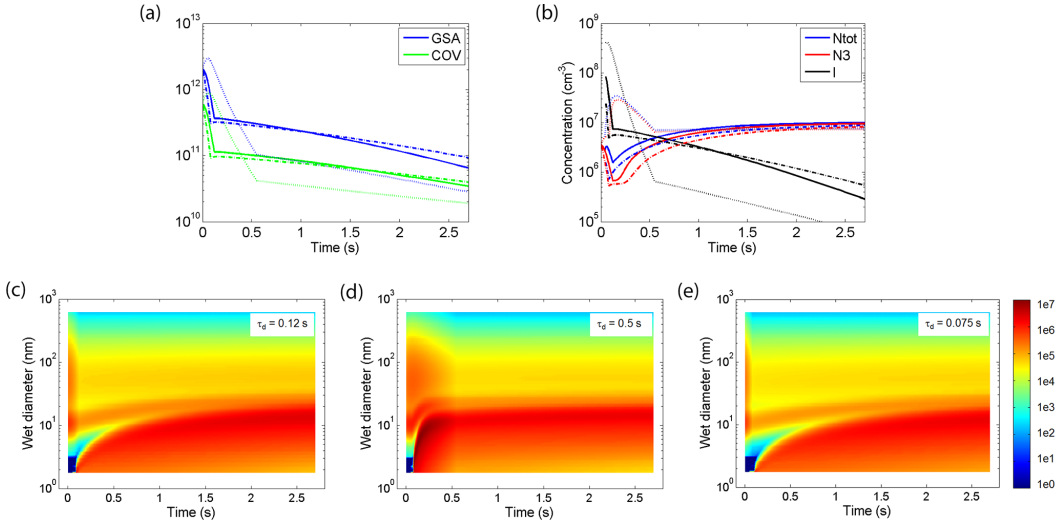

Figure 8. Effects of time constant (τ_d) on time evolution of gases **(a)**, particle number and nucleation rate **(b)** and number size distribution **(c–e)**, where particle number concentration in cm^{-3} is shown by color bar. In **(a)** and **(b)**, solid curves refer to τ_d = 0.12 s (base case), dotted curves to τ_d = 0.5 s, and dasdotted curves to τ_d = 0.075 s.

ACPD
15, 4219–4263, 2015

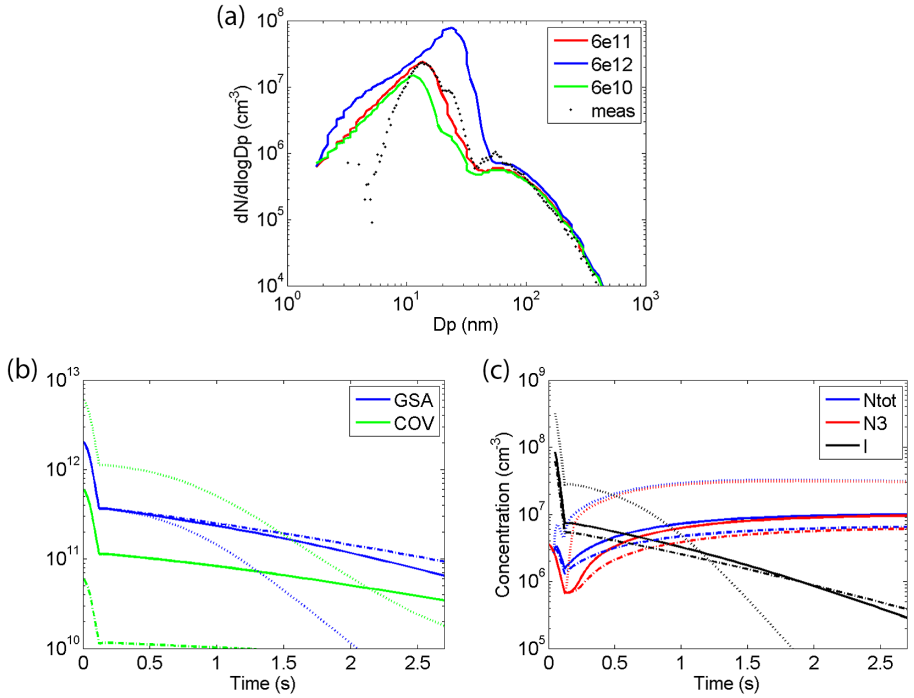

Figure 9. Number size distribution at the end of the simulation **(a)**, time evolution of gas concentrations **(b)**, time evolution of particle number concentration and nucleation rate **(c)** with the COV concentrations of 6×10^{10} (dashdot curves), 6×10^{11} (base case, solid curves), and 6×10^{12} (dotted curves) cm^{-3}.

ACPD
15, 4219–4263, 2015

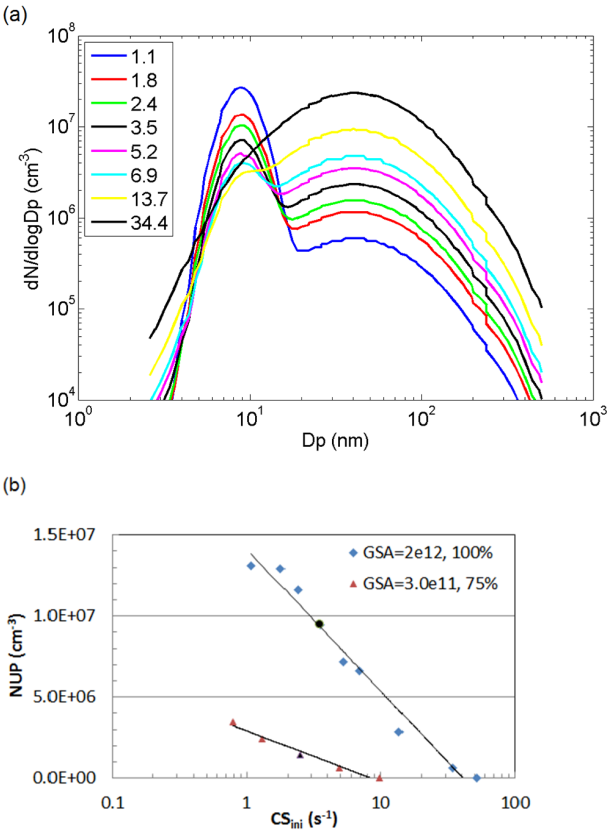

Figure 10. (a) Initial soot and core mode concentrations. The legend shows the corresponding condensation sinks in s^{-1}. **(b)** Nucleated particle concentration (NUP) at the end of the simulation as a function of initial condensation sink for 100 % engine load with GSA = 2×10^{12} cm^{-3} and raw exhaust T = 697 K. Also shown in **(b)** are the results for 75 % engine load with GSA = 0.3×10^{11} cm^{-3} and raw exhaust T = 657 K. Back dots refer to the base cases.

ACPD
15, 4219–4263, 2015

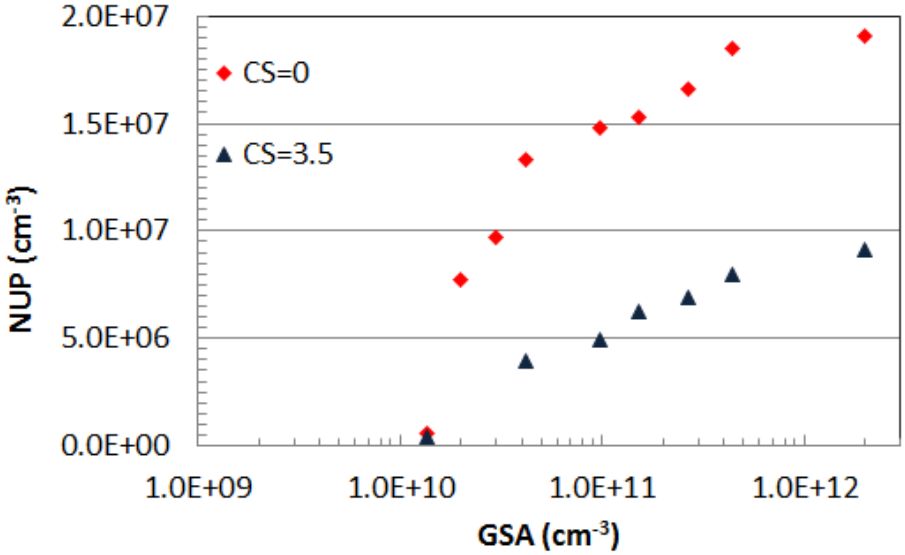

Figure 11. Nucleated particle concentration (NUP) at the end of the simulation as a function of initial GSA concentration for 100 % engine load. The initial core and soot mode concentrations were as in the base case (CS = 3.5 s^{-1}) or zero (CS = 0 s^{-1}).

ACPD
15, 4219–4263, 2015